Journal of Materials Chemistry A

Accepted Manuscript

ROYAL SOCIETY OF CHEMISTRY

www.rsc.org/materialsA

Journal Name

RSCPublishing

ARTICLE

3Cmite this: DOI: 10.1039/x0xx00000x

Received ooth January 2012,
Accepted ooth January 2012

DOI: 10.1039/x0xx00000x

www.rsc.org/

Pt/Single-stranded DNA/Graphene Nanocomposite with Improved Catalytic Activity and CO Tolerance

Mengzhu Li, Yuxia Pan, Xiaoyu Guo, Yinhua Liang, Yiping Wu, Ying Wen* and Haifeng Yang*

The Education Ministry Key Lab of Resource Chemistry Department of Chemistry Shanghai Normal University, Shanghai, 200234, P. R. China.

E-mail: hfyang@shnu.edu.cn (Haifeng. Yang); wenying117@hotmail.com (Ying. Wen)

The ssDNA could well-dispersed reduced graphene oxides (RGO) to form ssDNA-RGO composites, which could be used as superior support to expediently electrodeposit Pt to synthesize ssDNA-RGO/cotton-flower-like-Pt nanocomposites (ssDNA-RGO/cf-Pt). The formation of cotton-flower-like-Pt clusters was due to the assist of nitrogen atoms and phosphate groups in ssDNA. The catalytic activity of ssDNA-RGO/cf-Pt for methanol oxidation was 2.5 fold of RGO/Pt and 3.8 fold of commercial Pt NPs. The outstanding catalytic activity of such novel catalyst was attributed to huge surface of higher conductive ssDNA-RGO and cotton-flower-like-Pt clusters with an open structure. The latter was beneficial to mass transfer. In addition, the excellent ability of ssDNA-RGO/cf-Pt against CO poison was found and anti-poison ratio (If /Ib) of ssDNA-RGO/cf-Pt was of 1.75 larger than RGO/Pt and commercial Pt NPs. The elevated oxidation of CO in adsorption state should be from ssDNA providing abundant oxygen groups as well as the residual oxygen species in RGO. The possible mechanism for improved catalytic activity and CO tolerance was deduced according to UV-visible, Raman, SEM, EDS, XPS and CV results.

Introduction

The rapid increase of energy demand in people's daily life and quick consume of fossil fuel reserves concerned us, which also make human to anxiously face with a variety of environmental concerns.[1] Therefore, it is urgent to look for green and efficient energy sources to instead of fossil-based fuels. Nowadays, for the instance, proton exchange membrane fuel cells (PEMFCs), direct methanol fuel cells (DMFCs), and direct formic acid fuel cells (DFAFCs) have been extensively investigated for inspecting their possibility as the candidates of fossil fuel cell.

All the fuel cells are expected to be in the common characters of high energy density and low environmental pollution as compared to traditional energy sources. Amongst, methanol is regarded as one of the most appropriate fuels for the direct alcohol fuel cells, thanking to its low molecular weight, simplest structure, and very high energy density as well as low-cost,[2] perfectly meeting the actual needs for new energy. For promoting the practical application of alcohol-based fuel cells, the key point for the technical development focused on the designing novel and superior anodic catalysis materials as well as optimizing synthesis process.

As the matter of fact, platinum (Pt) shows the highest electrocatalytic ability for electro-oxidation of methanol oxidation reaction (MOR) on the anode among the metal catalysts. However, there are still unsolved problems, which largely limit the application of Pt in fuel cells .One severe barrier is the poisoning of CO towards the Pt electrode during MOR, due to CO tightly occupying active sites on the surface of catalyst.[3]

According to a previous research work,[4] oxygen-containing surface species (e.g., OH) formed on adjacent bimetallic catalyst sites could improve the ability to remove the adsorbed CO (CO_{ad}) from the catalyst surface. Based on this mechanism called bifunctional assay, a strategy is extended to synthesis alloy Pt with other oxophilic elements such as Pd[5], Ru[6], Sn[7], Au[8] and Fe[9], which offer abundant active sites for the adsorption of methanol and formation of OH specie. Papakonstantinou etc., in the observation of oxide graphene (GO) /Pt-based MOR, found that the presence of many oxygen groups on the surface of graphene could accelerate the oxidation of CO_{ad} at the active Pt sites.[10] Due to GO not a conductive support, GO/Pt-based catalyst exhibited an advantage of anti-poison of CO but the catalytic activity was inhibited to great extent. Alternatively, reduced graphene (RGO) with the greater surface to volume ratio (theoretically 2600 m^2g^{-1})[11] and well conductive feature[12]could also be used as carbon support to electrodeposite Pt catalyst. Moreover, residual oxygen species in RGO provide nucleation centres or sites for loading the catalysts.[13] In addition, lots of edges and defects on RGO assist in facilitating electron transport and accelerating mass transfer kinetics at the electrode surface to contribute to the high activity of Pt.[14]Furthermore, during the methanol oxidation process, RGO is simultaneously oxidized and the oxidation of the carbon supports is found to promote the Pt activity.

In the present work, we firstly try effort to respectively electrodeposit Pt onto the surfaces of GO and RGO dispersed by single-stranded DNA (ssDNA) to explore an optimization method for elevating catalytic activity of Pt nanocatalyst. As well known, ssDNA has much greater affinity to bind the graphene than the double-stranded DNA.[15] The possible reason is attributed to stronger interaction ssDNA with graphene basal plane through π–π stacking in its open structure.[16] Astonishingly, we found that ssDNA provided abundant oxygen groups, which could enhance the resistance of CO poison to catalyst. In turn, the nucleobase containing multiple nitrogen atoms in exocyclic amino group and imino group functional groups served as favourably defined sites for facilitating the formation of uniform cotton-flower-like Pt (cf-Pt) nanoparticles (NPs),[17] which eventually produced superior electrochemically active surface areas (ECSAs). Last but not least, while applied voltage range from −0.2~1.2 V, irreversible oxidative damage of guanine and adenine in ssDNA will be induced,[18] depleting oxygen produced in CH_3OH electro-oxidation and restraining the conversion of Pt to PtO in such reaction system. As an interesting finding, this proposed novel ssDNA-RGO/cf-Pt anode showed not only high catalytic activity for methanol oxidation but also an excellent CO tolerance.

Experimental

Materials

Hexachloroplatinic (IV) acid hexahydrate (H2PtCl6·6H2O), Trisodium citrate dihydrate (Na3C6H5O7, ≥99%), Graphite were purchased from Sinopharm Chemical Reagent (China).DNA. Fish Sperm DNA Sodium Salt (fsDNA) was purchased from Aladdin. Pt black were obtained from Sigma-Aldrich. Sodium chloride (NaCl, ≥99.5%) purchased from Shanghai RichJoint Chemical Reagent (China) all the chemicals and reagents were used as received. Ultrapure water (18.2 MΩ cm) was used throughout the experiments

Synthesis of DNA-modified RGO

Graphene oxides (GO) were prepared from graphite powder by the modified Hummer's method.[19] First of all, natural fsDNA (4mg, 5mg, 6mg or 7mg) was suspended in 10mL water and heated at 100 °C for 2 h to obtain ssDNA. After GO dispersion (1mg/ml, 5ml) was mixed with ssDNA solution, this mixture was reduced by sodium

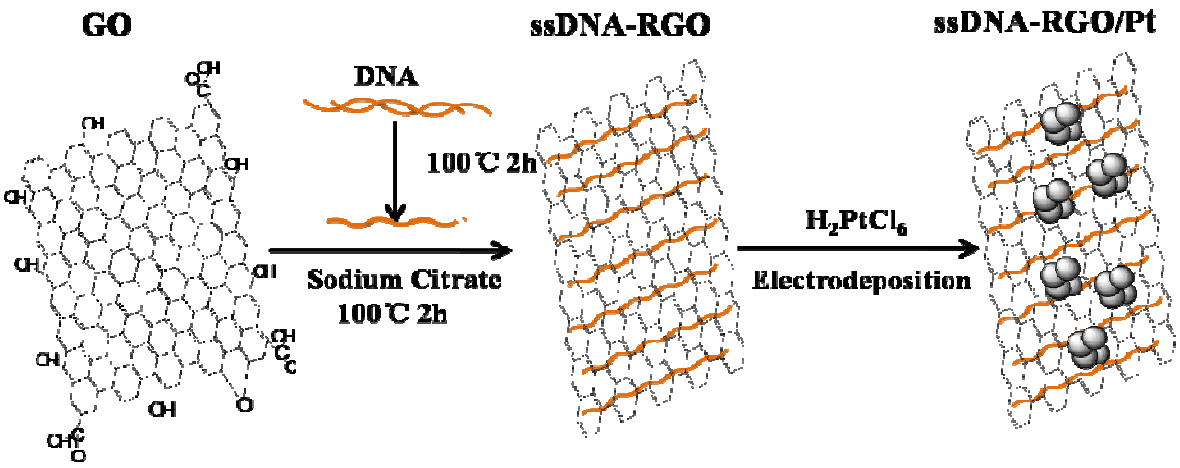

Scheme 1. Schematic Illustration of the procedure for preparing ssDNA-RGO/Pt Hybrid

citrate (1wt%, 2ml) for 2h under 100 °C. And then, NaCl (0.4675g, 50mM) was added in the suspension to remove the excess $Na_3C_6H_5O_7$ by several times centrifugation and double-distilled water rinsing. The resultant DNA-modified RGO solution (containing 0.5 mg/ml RGO) was shorted as ssDNA-RGO.

Modification of the anode

Before electrodeposition, the glassy carbon electrode (GCE) in diameter of 3 mm was polished by 0.3μm and 0.05 μm alumina powders followed by ultrasonicated sequentially in doubly distilled water, absolute ethanol and doubly distilled water for 3 min. Then, 10 μl ssDNA-RGO with different quantities of DNA were dropped onto the surface of GC electrode and then dried under an infrared lamp. The 10 μl aqueous solution of GO (0.5 mg/ml), GO (0.5 mg/mL) and ssDNA (6 mg/ml, 10 ml) were also immobilized onto the surface of GCE for control experiments.

The electrodeposition process was conducted at an optimized constant potential of -0.2 V in a solution containing 19 mM H_2PtCl_6 and 20 mM KCl and the deposited quantity of Pt ended at 5.052 μg through capacity evaluation. For a comparison, the commercial Pt-black modified GCE was also made by directly casting 10.0 μl aqueous Pt-black (0.5 mg·mL-1) onto a cleaned electrode surface and the amount of Pt kept same as electrodeposition case.

Electrochemical measurements

The electrochemical experiments were performed using a CHI660D potentiostat (Shanghai Chenhua Instrumental Co., Ltd., China) under ambient temperature in a cell, consisting of a modified GCE as a working electrode, an Ag/AgCl (in 3 M KCl solution) as the reference electrode, and a Pt wire as a counter electrode. Methanol oxidation reaction was

Scanning electron microscopy (SEM) and energy dispersive spectrometer (EDS) were carried out using Hitachi S-4800 Scanning electron microscopy. UV–vis spectra were recorded using a 760-CRT double beam ultraviolet-visible spectrophotometer (Shanghai Precision and Scientific Instrument Co., Ltd). Raman observation was done with a confocal microprobe Raman system (LabRam II, Dilor, France) and X-ray photoelectron spectroscopy (XPS; PHI 5000 VersaProbe) was used to identify the chemical composition of the surface of the resultant anode material.

Results and discussion

The procedure for preparing ssDNA-RGO/cf-Pt hybrid is shown in Scheme. 1. First of all, natural dsDNA was heated to obtain ssDNA at 100 °C for 2 h. And then, keeping the temperature at 100°C, GO dispersion was mixed with ssDNA and sodium citrate was injected to reduce GO into RGO for preparing ssDNA-RGO hybrid system.

The preparation process of ssDNA-RGO hybrid system was monitored using UV-vis spectroscopy. As showed in Fig. 1(A), a strong UV-vis absorption band for GO at 236 nm refers to π→π* transitions of C=C and a weak band around 300 nm is from n→π* transitions of C=O.[20] After reduction reaction, the absorption red-shift peak of ssDNA-RGO could be seen at 254 nm due to the restored electronic conjugation within graphene sheets. The digital photos of GO (pale brown), ssDNA-RGO (black), RGO (black) in water were also taken. Clearly in Fig. 1(B), ssDNA-RGO hybrid is dispersed in water in uniform way with long-term stability (> 3 months). Without ssDNA modification, pure RGO easily trends to aggregate and even precipitate after storage for one day. Similarly, the instable mixture of dsDNA-RGO also trends to agglomerate.

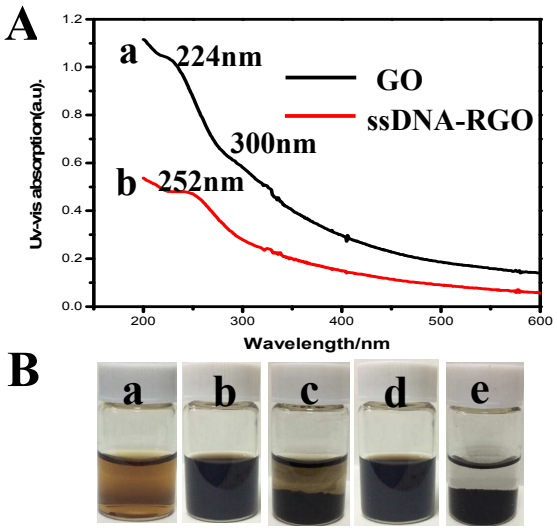

Fig. 1 (A) UV-vis absorption results of GO (a), ssDNA-RGO (b). (B)Optical photos of GO (a), ssDNA-RGO (b), RGO (c), ssDNA-RGO after three months (d), dsDNA-RGO (e)

Raman spectroscopy is considered a very efficient technique to certify structural changes of graphene.[21] In Fig. 2, two typical peaks at 1334and 1598 cm^{-1} of GO are ascribed to the D and G bands. The D band results from defects in the curved graphene sheet as an indication of disorder structures of GO and the G band is from the vibration of sp^2-bonded structures in a carbon 2D hexagonal lattice.[22] The D band and G band located in 1334 and 1598 cm^{-1} of RGO are same as both Raman bands of GO. The similar Raman results could also be observed in the electrochemical reduction of GO to form RGO [23] and the synthesis of RGO from GO by a chemical method using $NaBH_4$.[24]The normal Raman spectrum of pure graphite shows a typically sharp peak at 1580 cm^{-1}.Interestingly, both D and G bands of ssDNA-RGO observed at 1327 cm^{-1} and 1589 cm^{-1} are shifted, demonstrating that ssDNA-RGO system is successful architected through π–π interactions between single-stranded DNA and graphene basal plane.[25] The calculation of intensity ratio I_D/I_G can identify the degree of disorder of such carbon materials. The value of I_D/I_G (1.17) for ssDNA-RGO is larger than GO (1.01), RGO (1.07), which is attributable to the decrease in the average size of the sp^2.[26] Herein, ssDNA acts as an outstanding dispersant to improve the dispersion efficiency of RGO in water via π–π interactions.

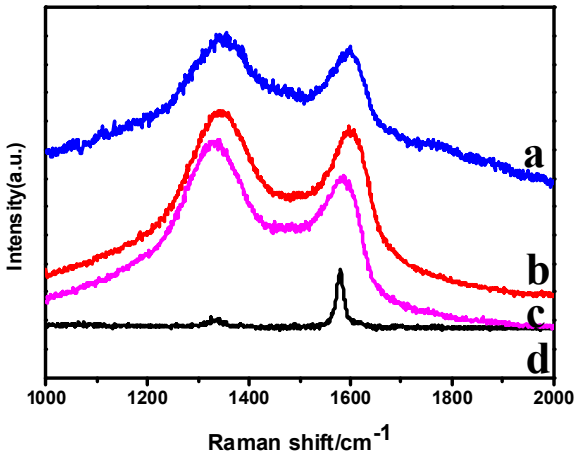

Fig. 2 Raman spectra of GO (a), RGO (b), ssDNA-RGO (c),Graphite (d).

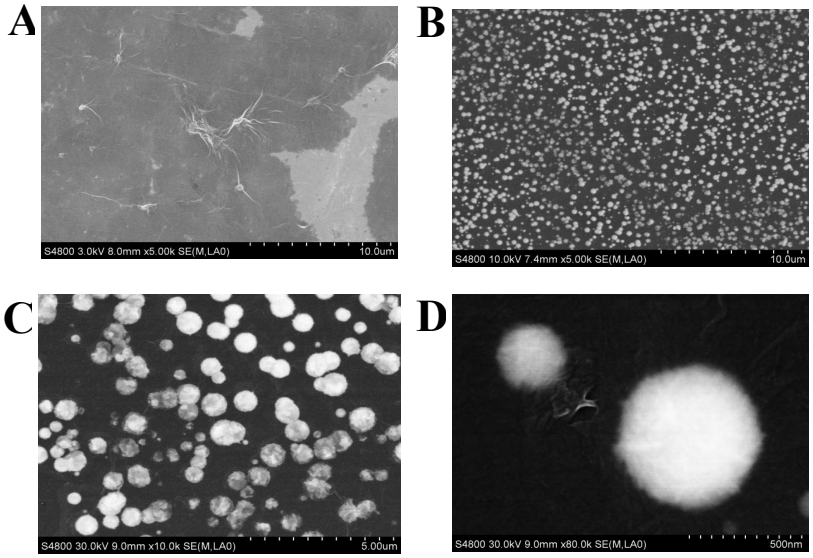

Fig. 3 SEM images of (A) ssDNA-RGO, (B-D) ssDNA-RGO/ct-Pt shown at different scales

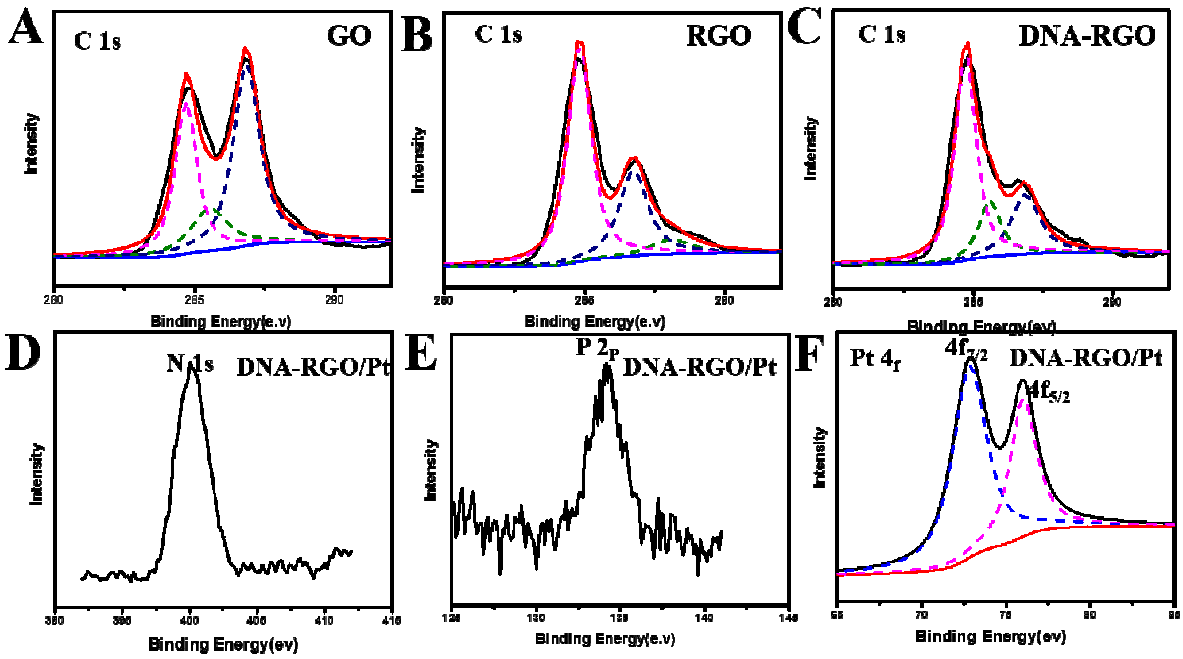

Fig. 4 XPS spectra of (A) carbon 1s of GO, (B) carbon 1s of RGO, (C) carbon 1s of ssDNA-RGO/cf-Pt, (D) nitrogen 1s of ssDNA-RGO/cf-Pt, (E) phosphorus 2p of ssDNA-RGO/cf-Pt, (F) platinum 4f of ssDNA-RGO/cf-Pt.

The electrodeposition of cf-Pt nanoparticles onto ssDNA-RGO modified GCE was investigated using SEM. The SEM image of ssDNA-RGO in Fig. 3(A) shows the typical lamellar structure of RGO with intrinsic rumples. Fig. 3(B) proves that the cf-Pt NPs are homogeneously deposited on the surface of RGO. The cf-Pt NPs in Fig. 3(C) could be ascribed to the favourable nucleation and defined electrodeposition sites along the DNA lattice provided by the exocyclic amino and imino groups in nucleobases. The clear image of cf-Pt NPs directly deposited on the crinkle of ssDNA-RGO in Fig. 3(D) exhibits the tight interaction between ssDNA and cf-Pt NPs. As a comparison experiment, when Pt NPs was electrodeposited on the surface of the pure RGO and GO, the corresponding SEM and TEM images shown in Fig. S1 depict the severe aggregation of the spherical Pt NPs at their surfaces. According to size statistic graphs in Fig.S2, the sizes of ssDNA-RGO/cf-Pt, GO/ Pt and RGO/ Pt are mainly in the ranges of 200~800 nm, 100~255 nm and 10~35 nm, respectively. Clearly, the cf-Pt clusters on ssDNA-RGO present the open structure, which could be expected to facilitate mass transfer process and elevate the active area of pt.

Table 1 Elemental Atomic Concentration from XPS Consequence

Sample	atomic concentration%					
	C	O	C/O	N	P	Pt
GO	65.40	34.60	1.89			
RGO	73.31	26.69	2.74			
ssDNA-RGO	64.87	35.13	1.85			
ssDNA-RGO/cf-Pt	62.30	33.74	1.85	3.22	0.74	0.034

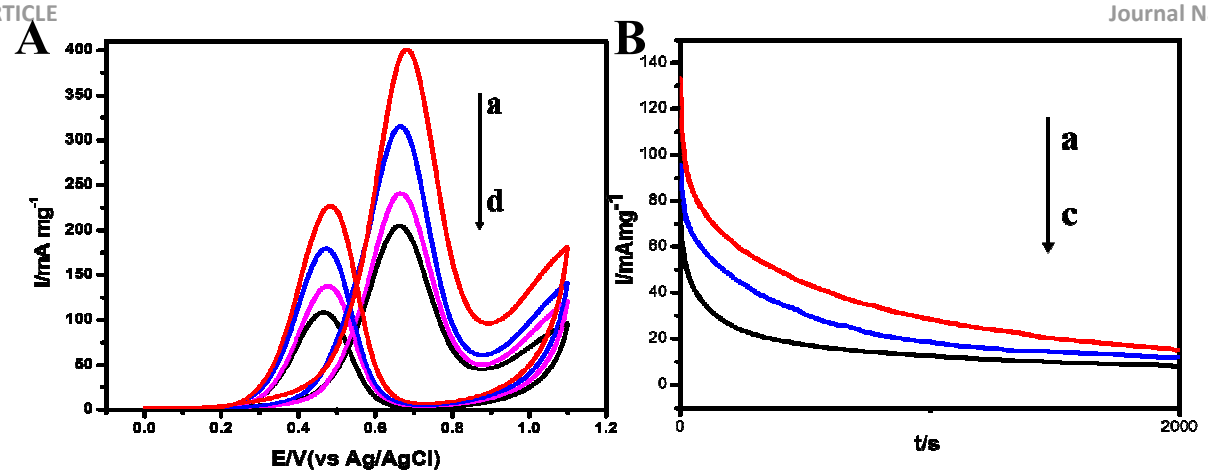

Fig. 5 (A) CVs of ssDNA –RGO/cf-Pt with 6mg DNA(a), 5mg DNA (b), 4mg DNA(c), 7mg DNA(d) in 0.5 M H_2SO_4 +1 M CH_3OH at the scan rate of 50 mVs^{-1}, (B) Chronoamperometry curves of ssDNA (6mg)-RGO/Pt(a), RGO/Pt (b),pure Pt (c) in 0.5 M H_2SO_4 +1 M CH_3OH at 0.6 V.

In Fig. 4(A), XPS analyze for the surface fictionalization of GO, RGO, and ssDNA-RGO, provides the composition information. For GO sheets, the fitted C_{1s} peaks located at 284.7 eV, 285.6 eV and 286.8 eV were corresponding to C=C/C-C bond, C−OH and C−O−C bond,[27] respectively. While GO was reduced to RGO, with the loss of oxygen moieties it generated new sp^2 C−C bond. Correspondingly in Fig. 4(B) for XPS of RGO, a peak from C−OH is disappeared and a new peak of C=O is observed. In turn, the increasing intensity of C=C/C−C can be easily found in the spectral range of 285.5 eV−289.0 eV. After the formation of ssDNA-RGO, in Fig. 4(C), the novel peak at 286.2 eV is related to C−N of ssDNA.[28] XPS data of Nitrogen 1s (400.2 eV) and phosphorus 2p (134.3 eV) in Figs. 4(D) and 4(E) also confirm the successful modification of ssDNA on the surface of RGO. In addition, O_{1s} XPS peak of GO locates at 532.6 eV and for RGO, O_{1s} XPS peak red shifts to 532.8 eV as shown in Fig. S3 while two O_{1s} XPS peaks of ssDNA-RGO present at 532.6 eV and 535.9 eV. The latter peak located in 535.9 eV may be contributed to O elements in ssDNA. As shown in XPS spectrum of Pt in ssDNA-RGO/cf-Pt of Fig. 4(F), the positive shifts of both peaks referring to Pt $4f_{7/2}$ and Pt $4f_{5/2}$ happen to be seen at 72.8 and 76.1 eV, comparing to the XPS bands of metallic Pt at 71.4 (Pt $4f_{7/2}$) and 74.6 eV(Pt $4f_{5/2}$).[29]The possible reason is that the shifts of both binding energies of Pt might indicate the strong interaction of Pt with heteroatoms in ssDNA-RGO system especially nitrogen and phosphate moieties in ssDNA after carefully comparing with the XPS bands of nitrogen 1s at 400.5 eV and phosphorus 2p at 133.6 eV, given in literature.[30] EDS results shown in Fig. S4 also marks the presence of N, Pt, O and C and further verifies successful formation of ssDNA-RGO/cf-Pt.

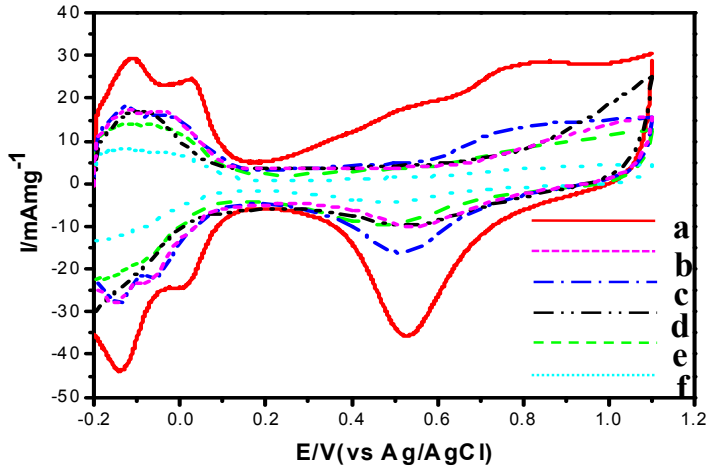

Fig. 6 CVs of ssDNA (6mg)-RGO/cf-Pt (a), RGO/Pt (b), GO/Pt (c), pure Pt (d), ssDNA/P t (e) and ssDNA (6mg)-GO/Pt (f) in 0.5 M H_2SO_4 with scan rate of 50 mV s^{-1} .

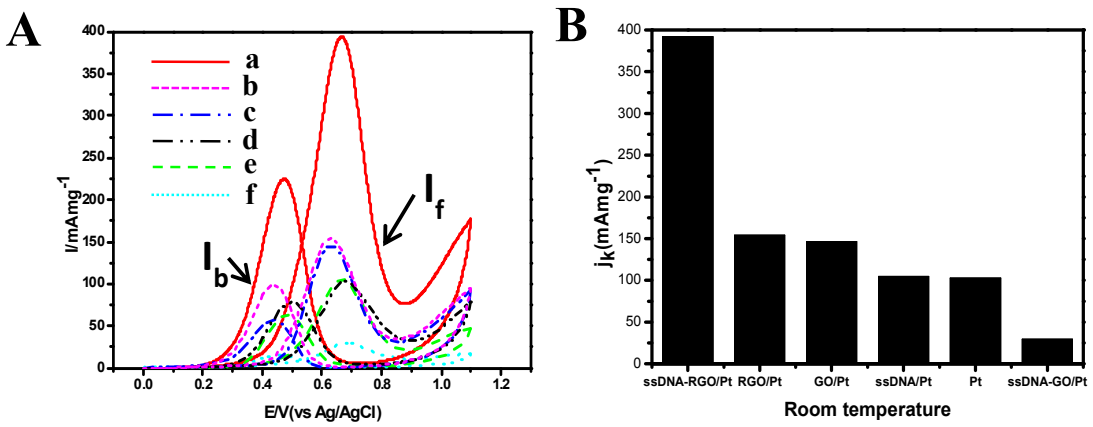

Fig. 7 (A)CVs of ssDNA (6mg)-RGO/cf-Pt (a), RGO/Pt (b), GO/Pt (c), pure Pt (d), ssDNA/Pt (e) and ssDNA (6mg)-GO/Pt(f) in nitrogen saturated aqueous solution of 0.5M H_2SO_4, scan rate 100mVs^{-1}. (B) Mass activity of different catalysts with the kinetic current density (j_k) normalized referred to the loading amount of Pt.

As showed in Fig. 5(A), through the observation of the change of CVs with the increase of amount of DNA from 4 mg to 7 mg, the superior catalytic activity of ssDNA-RGO/cf-Pt for methanol electro-oxidation than the other could be found when 6 mg DNA is used. The durability and long–term activity of DNA-RGO/cf-Pt within 2000 s shows better than commercial Pt NPs and RGO/Pt as shown in Fig. 5(B)

The electrochemical behaviours of the resultant ssDNA–RGO/cf-Pt, RGO and commercial Pt modified GCEs were observed using Cyclic voltammetry (CV) method in nitrogen saturated 0.5 M H_2SO_4 aqueous solution at a potential scan rate of 100 mV s^{-1} (Fig. 6). ECSA (active surface area) can be calculated by measuring the columbic charge collected in hydrogen adsorption and desorption region between -0.2~0.1 V. According the following equation, [31] ECSAs=Q_H/m·C (setting that 0.21 mC cm^{-2} charge is required to oxidize a monolayer of H_2 on the surface of Pt, and m refers to the platinum loading), ECSAs of commercial DNA-GO/Pt, DNA/Pt, Pt NPs, RGO/Pt, GO/Pt and DNA-RGO/cf-Pt were 11.8 m^2 g^{-1}, 40.1 m^2 g^{-1},96.8 m^2 g^{-1}, 95.3 m^2 g^{-1}, 112.3 m^2 g^{-1}, and 234 m^2 g^{-1}, respectively. The greater ECSA shows the more catalytically active sites available for electrochemical reaction and simultaneously reflects the conductive pathway available at the surface of electrode for transfer electrons, which is contributed from the open structure of cotton-flower Pt clusters formed by the aid of ssDNA and the huge surface area of RGO. Therefore, the existence of ssDNA in DNA-RGO/cf-Pt is also a key factor to improve the catalytic activity of Pt.

According to Fig. 7(A), the optimal ssDNA-RGO/cf-Pt modified GCE exhibits the highest current density (1.98 mA cm^{-2}), which is 2.5 fold of RGO/Pt and 3.8 fold of commercial Pt NPs. Corresponding to Fig. 7(B), mass activity of DNA-RGO/cf-Pt is 391.9 mAmg^{-1}, while commercial Pt NPs is only 99.6 mA mg^{-1}, RGO/Pt is 154.1 mA mg^{-1}, GO/Pt is 140.4 mA mg^{-1}, ssDNA/Pt is 154.1 mA mg^{-1} and ssDNA-GO/Pt is 28.5 mA mg^{-1}.

It should be mentioned that the optimal ssDNA-RGO/cf-Pt GCE possesses both the highest electrocatalytic activity and superior CO tolerance capability but the case of GO/Pt. The difference between GO and RGO lies in the amount of oxygen groups. As above described, GO sheets with abundant oxygen groups have better anti-poison ability. The forward anodic peak around 0.7V marked as I_f refers to the oxidation of methanol and the backward anodic peak around 0.5V marked as I_b refers to the oxidation of COads-like species.[32] The ratio of I_f/I_b represents the CO tolerance ability of catalysts. In Table 2, the I_f/I_b ratio of GO/Pt at 2.56 is larger than 1.56 of RGO/Pt. Considering the atomic concentration in Table 1, the carbon/ oxygen ratio of GO is 1.89, which is smaller than 2.74 of RGO. Unfortunately, GO sheets are not good conductivity, hindering the electron transport rate as well as resulting in the decrease of its catalytic ability as shown in Fig. 7(B). The smallest carbon/oxygen ratio of ssDNA-RGO is evaluated about 1.85 on the basis of the XPS result tabulated in Table 1. However, the I_f/I_b of ssDNA-RGO/cf-Pt is 1.75, showing that the ability of ssDNA-RGO/cf-Pt against CO is not in the best position of Table 2. This phenomenon might be due to its excellent catalytic activity generating more CO species during methanol oxidation process to occupy the active sites of Pt Comparing with the case of RGO/Pt, nitrogen functional groups in ssDNA-RGO/cf-Pt from ssDNA play the role in not only producing cotton-flower-like Pt with an enhanced electroactivity but also in adsorbing water to produce OH adsorption onto ssDNA-RGO/cf-Pt

Table 2 Comparison of anti-poison ability of different catalyst

Catalyst	I_f	I_b	I_f/I_b
Pt	**0.52**	**0.39**	**1.33**
RGO/Pt	**0.78**	**0.5**	**1.56**
GO/Pt	**0.74**	**0.29**	**2.56**
ssDNA/Pt	**0.53**	**0.32**	**1.67**
ssDNA (6mg)-GO/Pt	**0.15**	**0.07**	**2.14**
ssDNA (6mg)-RGO/cf-Pt	**1.98**	**1.14**	**1.75**

surface, which should greatly contribute to the resistance of CO-poisoning. What's more, OH groups in phosphate backbone of ssDNA as a Pt formation site (see Figure 7A) might also contribute improvement for the CO tolerance of DNA-RGO/cf-Pt. As above proposed, the CO tolerance of DNA-GO/Pt should be the best, but the I_f/I_b ratio of DNA-GO/Pt at 2.14 is smaller than that of GO/Pt. It is contributed to the DNA reduces the oxygen groups of GO in the snythesis process of DNA-GO hybrid.[33] Obviously in Table 2, without RGO, ssDNA/Pt is poor catalytic ability due to its non-conducting characteristic. The proposed mechanism is described in the following equations:

$$\text{RGO-ssDNA}+H_2O \rightarrow \text{RGO-ssDNA-}(OH)_{ads}+H^+ + e^-$$

$$\text{RGO-ssDNA-}(OH)_{ads}+\text{cf-Pt/}CO_{ads} \rightarrow CO_2+\text{RGO-ssDNA}+H^+ + e^-$$

Conclusion

We successfully employed ssDNA to well disperse graphene oxides in water and then added reduction regent to synthesize ssDNA-RGO composites. The ssDNA-RGO modified CGE with huge surface area and nice conductivity, was easily deposited Pt nanoparitcles onto the surface. Due to the presence of nitrogen sites and phosphates moieties in ssDNA, the Pt nanoparitcles presented cotton-flower-like structure, exhibiting high catalytic activity for methanol oxidation. Oxygen residual species (e.g., OH) on the surface of RGO and OH species formed from water caught by nitrogen functional groups in ssDNA could accelerate the oxidation of CO_{ad}, which are beneficial to improving CO_{ad} removal. Therefore, ssDNA-RGO/cf-Pt catalyst showed an advantage of inhibition of CO poison to greater extent. We found the ssDNA played a vital role in not only well-dispersion of RGO as the support for the formation of open structure of Pt with high activity, but also the enhancement of its CO tolerance.

Acknowledgements

This work is supported by the National Natural Science Foundation of China (No.21475088), PCSIRT (IRT1269) and International Joint Laboratory on Resource Chemistry (IJLRC), Shanghai Key Laboratory of Rare Earth Functional Materials, and Shanghai Municipal Education Committee Key Laboratory of Molecular Imaging Probes and Sensors.

References

1 M. Armand,J. M. Tarascon, *Nature*, 2008, **451**, 652-657.

2 M. M. Liu, R. Z. Zhang, W. Chen,*Chem. Rev*, 2014, **114**, 5117-5160.

3 J. M. Leger, *J. Appl. Electrochem*, 2001, **31**, 767-771.

4 F. McBride, G. R. Darling, K. Pussi, C. A. Lucas, Y. Grunder, M. Darlington, A. Brownrigg, A. Hodgson, *J. Phys. Chem. C*, 2013, **117**, 4032−4039.

5 S. J. Guo, S. J. Dong, E. K. Wang, *ACS Nano*, 2010, **4**,547–555.

6 S. Y. Bong, Y. R. Kima, I. Kima, S. H. Woo, S. H. Uhmb, J. Y. Lee, H. Kima, *Electrochemistry Communications*, 2010, **12**, 129–131.

7 V. R. Stamenkovic, M. Arenz, C. A. Lucas, M. E. Gallagher, P. N. Ross, N. M. Markovic, *J. Am. Chem. Soc*, 2003, **125**, 2736−2745.

8 Y.J. Hu, H. Zhang, P. Wu, H, Zhang, B. Zhou, C. X. Cai, *Phys. Chem. Chem. Phys*. 2011, **13**, 4083–4094.

9 W. Chen; J.M. Kim; S.H. Sun; S. W. Chen, *Langmuir* 2007, **23**, 11303–11310

10 (a) S. Sharma, A. Ganguly, P. Papakonstantinou, X.P. Miao, M. X. Li, J. L. Hutchison, M. Delichatsios, S. Ukleja, *J. Phys. Chem. C*. 2010, **114**, 19459–19466; (b) I. Fampiou, A.Ramasubramaniam, *J. Phys. Chem. C*, 2012, **116**,6543-6555; (c) A. Ambrosi, M. Pumera,*Chem. Eur. J*, 2010, **16**, 10946–10949.

11 Y. X. Liu, X. C. Dong, P. Chen, *Chem. Soc. Rev*, 2012, **41**, 2283–2307.

12 N. Zhang, Y.H. Zhang, Y. J. Xu, *Chem. Soc. Rev,* 2014, **43**, 8240-8254.

13 (a) M.Q. Yang, X.Y. Pan, N. Zhang, Y. J. Xu, *CrystEngComm,* 2013, **15**, 6819-6828; (b) R. Kou, Y. Y. Shao, D. H. Mei, Z. M. Nie, D. H. Wang, C. M. Wang, V. V. Viswanathan, S. Park, I. A. Aksay, Y. H. Lin, Y. Wang, J. Liu, *J. Am. Chem. Soc*. 2011, **133**, 2541–2547.

14 N. Zhang, Y.H. Zhang, Y. J. Xu, *Nanoscale,* 2012, **4**, 5792-5813

15 (a) J. N. Tiwari, K. C. Kemp, K. Nath, R. N. Tiwari, H. G. Nam, K. S. Kim, *ACS Nano*, 2013, **7**, 9223–9231; (b) J. N. Tiwari, K. Nath, S. Kumar, R. N. Tiwari, K. C. Kemp, N. H. Le1, D. H. Youn, J. S. Lee, K. S. Kim, *Nature Communication* 2012, **486**, 43–51; (c) W.Lv,M. Hui. Liang, F. M. Jin, L. Cui, L. J. Zhi, Q. H. Yang, *J. Mater. Chem*, 2010, **20**, 6668–6673.

16 (a) V. Georgakilas, M. Otyepka, A. B. Bourlinos, V. Chandra, N. Kim; K. C.Kemp, P.Hobza, R. Zboril, K. S.Kim, *Chem. Rev*. 2012, **112**, 6156-6214; (b) A. J. Patil, J. L. Vickery, T. B. Scott, S. Mann, *Adv. Mater,* 2009, **21**, 3159−3164.

17 K. Qu, L. Wu, J. S. Ren, X.G. Qu, *ACS .Appl. Mater. Interfaces*, 2012, **4**, 5001−5009.

18 (a) I. V. Yang, H. H. Throp, *Inorg. Chem*, 2000, **39**, 4969−4976; (b) M. E. Napier, D. O. Hull, H. H. Throp, *J. Am. Chem. Soc*, 2005, **127**, 11952−11953.

19 (a) G. T. Liu, H. F. Chen, G. M. Lin, P. P. Ye, X. P. Wang, Y. Z. Jiao,X. Y. Guo, Y. Wen, H. F. Yang, *Biosens. Bioelectron*, 2014, **56**, 26–32; (b) W. S.Hummers, R. E. Offeman, *J. Am. Chem. Soc*, 1958, **80**, 1339−1339,(c) M.Q.Yang,Y.J. Xu*, Phys. Chem. Chem. Phys,* 2013, **15**, 19102-19118.

20 M. M. Liu, R. Liu, W. Chen, *Biosens. Bioelectron*, 2013, **45**, 206-212.

21 J. C. Chaco ´ n-Torres, L. Wirtz, T. Pichler, *ACS Nano*, 2013, **7**, 9249–9259.

22 M. M. Zhang, J. M. Xie, Q. Sun, Z. Yan, Min,Chen, J. J. Jing, *Int. J. Hydrogen Energy*, 2013, **38**, 16402-16409.

23.Y.Y Jiang, Y.Z. Lu, F.H. Li , T.S. Wu, L. Niu, W.Chen, *Electrochem. Commun,* 2012, **19**, 21–24.

24 M. Y. Yen, C. C. Teng, M. C. Hsiao, P. I. Liu, W. P. Chuang, C. C. M. Ma, C. K. Hsieh, M. C. Tsai, C. H. Tsai, *J. Mater. Chem*, 2011, **21**, 12880–12888.

25 S. Stankovich, D. A. Dikin, G. H. B. Dommett, K. M. Kohlhaas, E. J. Zimney, E. A. Stach, R. D. Piner, S. T. Nguyen, R. S. Ruoff, *Nature*, 2006, **442**, 282–286. 22 C. H. Hsu, H. Y. Liao, Y. F. Wu, P. L. Kuo, *ACS. Appl. Mater. Interfaces*, 2011, **3**, 2169–2172.

26 C. H. Hsu, H. Y. Liao, Y. F. Wu, P. L. Kuo, *ACS. Appl. Mater. Interfaces*, 2011, **3**, 2169–2172.

27 W. Y.Kim,K. S. Kim, *Nat. Nanotech*, 2008, **3**, 408–412.

28 J. P. Avinash, L. V. Jemma, B. S. Thomas, M. Stephen, *Adv. Mater*, 2009, **21**, 3159–3164.

29 V. Singha, D. Jounga, L. Zhai, S. Das, S. I. Khondaker, S. Seal, 2011, 56, 1178–1271.

30 D. A.Stevens, M. T. Hicks, G. M. Haugen, J. R. Dahn, J. *Electrochem. Soc*, 2005, **152**, 2309–2315.

31 B.Lim, M. Jiang, P. H. C. Cama, E. C. Cho, J. Tao, X. Lu, Y. Zhu, Y. Xia, *Science*, 2009, **324**, 1302–1305.

32 L. Gao, W. Yue, S. S. Tao, L. Z. Fan, *Langmuir*, 2013, **29**, 957−964.

33 A. A. Kornyshev, *Phys. Chem. Chem. Phys*, 2010, **12**, 12352–12378

TOC

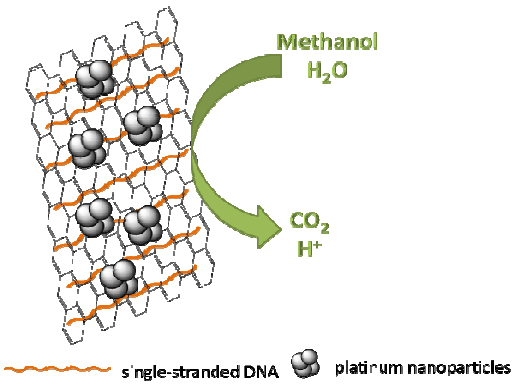

The ssDNA-dispersed RGO offered large electrochemical active surface to from cotton-flower-like-Pt(cf-Pt). ssDNA-RGO/cf-Pt showed highly catalytic activity due to Pt clusters with an open structure and promising ability against CO poison. The CO tolerance of such composites may be attributed to abundant OH induced by nitrogen atoms in ssDNA and oxygen species in ssDNA as well as the residual oxygen species in the surface of RGO.